



# Single underwater image enhancement by attenuation map guided color correction and detail preserved dehazing

Zheng Liang<sup>a,1</sup>, Yafei Wang<sup>a,1</sup>, Xueyan Ding<sup>a</sup>, Zetian Mi<sup>a</sup>, Xianping Fu<sup>a,b,\*</sup>

<sup>a</sup>Information Science and Technology School, Dalian Maritime University, Dalian 116026, China

<sup>b</sup>Pengcheng Laboratory, Shenzhen, Guangdong 518055, China

## ARTICLE INFO

### Article history:

Received 19 September 2019

Revised 24 March 2020

Accepted 27 March 2020

Available online xxx

Communicated by Dr. Ma Jiayi

### Keywords:

Underwater image enhancement

Color correction

Wavelength attenuation

Maximum intensity prior

Gradient domain

## ABSTRACT

The attenuation (sum of absorption and scattering), which caused by the dense and non-uniform medium, generally leads to problems of color degradation and detail loss in underwater imaging. To address these problems, we propose a systematic underwater image enhancement method, which includes an attenuation map guided underwater image color correction approach and a detail preserved dehazing approach. The color correction approach fully considers the main causes of color degradation in underwater imaging, namely wavelength-dependent attenuation of different colors. According to the attenuation map of each color channel, a piece-wise linear transform is used to process the information of each color channel. Then, the detail preserved dehazing approach based on multi-scale decomposition is proposed to compensate for the lost details while eliminating the effects of haze. Especially, an adaptive Maximum Intensity Prior (MIP) measurement based on maximum attenuation identification is proposed to estimate transmission of the medium. Experiments on a variety types of degraded underwater images have proven that our proposed method can produce accurate results with vivid color and fine details, even better than other state-of-the-art underwater image dehazing methods.

© 2020 Published by Elsevier B.V.

## 1. Introduction

It is an important subject to capture clear images in underwater environment for oceanic applications, such as underwater vehicles, oceanic engineering and marine biology. However, underwater images often show some degradation effects such as color casts, blurriness and poor detail. In underwater imaging, as light travels in the water, it is exponentially attenuated through two processes: absorption and scattering. The absorption is caused by the medium of water that degrades the energies of light rays according to their wavelengths with depth, which makes the image visually generating color distortion. The scattering effect is brought by the suspended particles in the water that reflect the light rays into other directions, which makes the image blurry. Therefore, underwater image color correction and detail enhancement have become a research hot spot in a wide range of applications.

Unfortunately, most existing dehazing techniques underperform in color restoration and detail enhancement. In terms of

color restoration, most of color correction methods used in land-based image are directly applied to correct underwater images, without considering the difference between land-based image and underwater image in color degradation. A major difference between light propagation in the atmosphere and in natural waters is wavelength dependent attenuation. Absorption in the atmosphere is generally negligible, but in the water its magnitude can be comparable to. At the same time, among the dehazed results generated by the existing methods, detail enhancement is not easily observable. There are two reasons for this: on the one hand, these state-of-the-art dehazing works assume that the attenuation of light under water is constant (e.g., red light is attenuated at the highest rate, blue light is attenuated at the slowest rate), and tend to make coarse airlight/transmission estimations. But the attenuation parameters are affected by seasonal, geographic, and climate variations. On the other hand, these dehazing methods based on image formation model (IFM) only consider the effect of ideal single scattering caused by particles, but in underwater, the effect of multiple scattering is inevitable and significant. Therefore, an effective underwater image dehazing method that can tackle these added problems for both color correction and detail enhancement is meaningful, and thus desired.

In this paper, we attempt to overcome these challenges by designing a novel underwater image dehazing methods combining

\* Corresponding author.

E-mail addresses: [zliang@dltmu.edu.cn](mailto:zliang@dltmu.edu.cn) (Z. Liang), [wangyafei@dltmu.edu.cn](mailto:wangyafei@dltmu.edu.cn) (Y. Wang), [dingxueyan@dltmu.edu.cn](mailto:dingxueyan@dltmu.edu.cn) (X. Ding), [mizetian@dltmu.edu.cn](mailto:mizetian@dltmu.edu.cn) (Z. Mi), [fxp@dltmu.edu.cn](mailto:fxp@dltmu.edu.cn) (X. Fu).

<sup>1</sup> Contributed equally to this work.

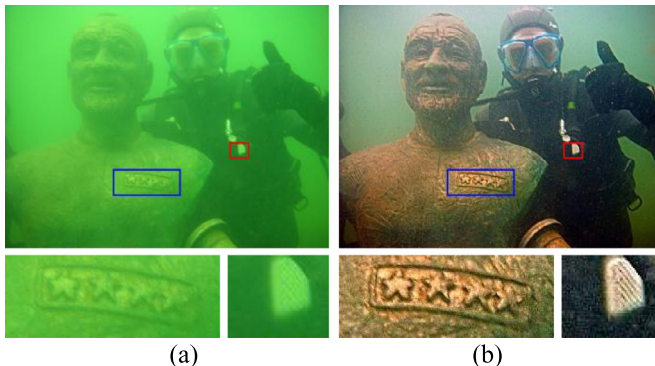


**Fig. 1.** Dehazed result generated by the proposed method. (a) Original underwater image. (b) Dehazed image.

color correction and detail enhancement. The proposed method can effectively remove the color cast and enhance the detail of underwater images captured in various conditions (Fig. 1). We summary the specific contributions as follows:

- An effective attenuation map guided color correction method is proposed to remove the color cast of underwater images. It takes into account the significant attenuation difference between R, G, and B channels, thereby introducing the attenuation level into underwater image color correction, which can pertinently process each channel based on a piece-wise linear transform.
- An underwater image dehazing method is presented, which consists of two steps: descattering in the base layer and detail enhancement in the different residual detail layers. Especially by applying the domain knowledge in base layer, scattered light caused by particles can be appropriately reduced and more structure information can be displayed. Extensive experiments demonstrate that the proposed method has desirable perception and clearer details.
- An adaptive MIP method is proposed to estimate the transmission of the medium based on maximum attenuation identification. Instead of making any assumption (e.g., red channel attenuates much faster or blue channel attenuates much faster), we use the maximum attenuation identification to select the color channel that attenuates at the highest rate in the image, which helps the MIP method to robustly estimate the transmission for images taken under various underwater environment.

The flowchart of the proposed method is illustrated in Fig. 2. The rest of the paper is organized as follows. In Section 2, we review the previous works related to the underwater image color correction and enhancement. The proposed single underwater image color correction and detail preserved dehazing methods are described in Section 3. Section 4 reports the experimental results. Finally, a conclusion about this paper is summarized in Section 5.

## 2. Related work

Recently, various methods involving underwater image dehazing and color correction have been proposed to tackle the poor visibility and color cast of underwater image.

Underwater image dehazing. Most existing underwater dehazing techniques can be described from two perspectives. One is the dehazing method that corresponds to restore the degraded images relying on the image formation model (IFM). Most methods using IFM have been inspired by the Dark Channel Prior (DCP) that was employed to dehaze images captured by the atmosphere. The DCP was originally intended to recover the images taken in outdoor scenes, it assumes that the object radiance of at least one

color component in a natural scene is close to zero. For instance, Chiang and Chen removed the haze and color variations by combining the DCP algorithm with the wavelength dependent compensation algorithm [1]. This method was perform well in enhancing the underwater images with bluish tone and removing the effects of artificial light. But it is limited when enhancing the underwater images with serious color distortion. Wen et al. [2] enhanced the underwater image via a new underwater optical model based on DCP. Galdran et al. [3] proposed a red channel prior method to enhance the underwater degraded images. Underwater Dark Channel Prior (UDCP) method was proposed by Drews et al. [4] to estimate the transmission of underwater scenes. They obtained an improved transmission than the conventional DCP. In addition, according to the fact that there is a large difference in attenuation among three image color channels under water, Carlevarisbianco et al. [5] designed the MIP method to estimate the transmission. Unfortunately, in most cases, these methods that based on the DCP and MIP cannot get desired restoration results on account of the varying lighting conditions in underwater imaging. To obtain satisfactory results, Peng and Cosman [6] adopted a method based on image blurriness and light absorption to estimate scene depth of underwater images. Li et al. [7] used the minimum information loss principle and histogram distribution prior to recover the lost contrast of underwater images, and Wang et al. [8] proposed an underwater image restoration method based on adaptive attenuation-curve prior, but the restored results generated by these methods have obvious reddish color shift and artifacts.

Another is the image enhancement technique based on the non-IFM, including the histogram-equalization-based methods, white balance, retinex-based and fusion-based approaches. For instance, Ghani et al. [9] applied a histogram stretching method to enhance the contrast of underwater images. Ancuti et al. [10] reconstructed a clear image via blending multiple images derived from the original image in multi-scale fusion strategy. Later, the previous work is modified for improving the color of resultant images and reducing the effects of over-exposure [11]. In [12], Fu et al. presented a method to enhance underwater images, which is based on the retinex theory [13]. The original image is decomposed into reflectance and illumination components by using a variational framework, and the enhanced image can then be obtained by combining the enhanced reflectance and the enhanced illumination.

Recently, the deep learning technique has made a great advance in the applications of computer vision. In [14], deep neural network has been proposed to remove the color shift and enhance the contrast. Later, Li et al. [15] proposed a semi-supervised learning network for underwater image restoration, namely WaterGAN. Since it needs to be trained via a large annotated dataset of images of pairs when applying the WaterGAN to restore underwater images, it is not feasible in processing the underwater images captured under unknown sites. Anwar et al. [16] developed a novel network framework called UWCNN. UWCNN is trained by a synthetic underwater image dataset that were produced in the indoor environment, and the clear underwater image can be reconstructed using UWCNN. More recently, a multiscale dense GAN is proposed to enhance the underwater images by Guo et al. [17], but the limitations of multiple possible outputs from GANs still cannot avoid. Compared with the IFM-based methods, these approaches are usually easier to implement. However, results yielded by these enhancement techniques may look visually unnatural (like oversaturation or over-enhancement).

**Color correction.** Most of the methods used to balance the image colors estimate the color of the light source by making a specific assumption [18], and then achieve color constancy by dividing each color channel by its corresponding normalized light source in-

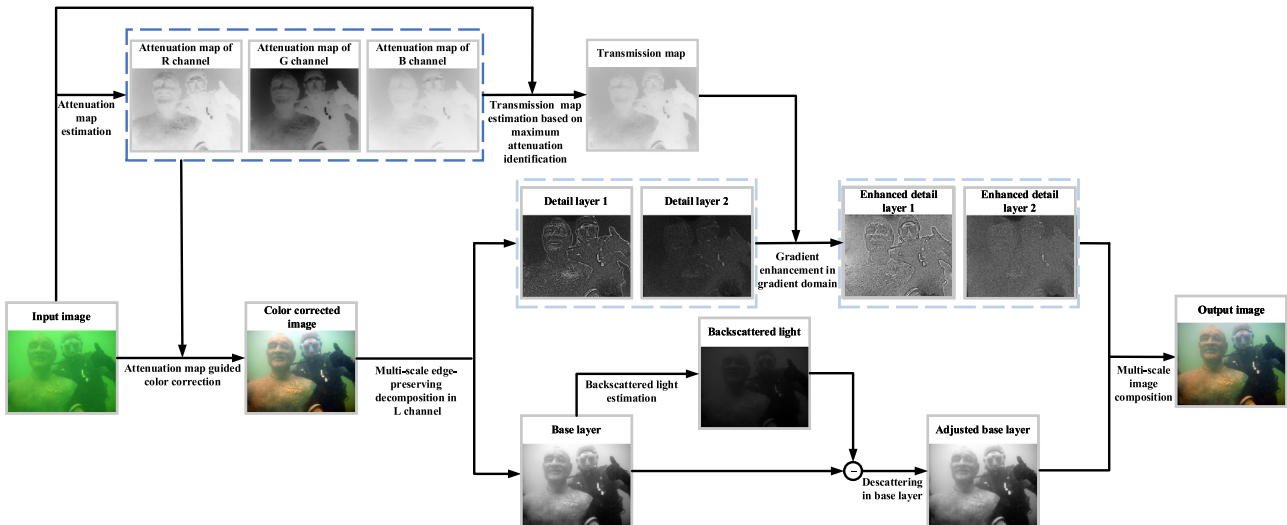


Fig. 2. The overview of the proposed method.

tensity. Among these methods, Buchsbaum [19] proposed the Gray world algorithm based on the assumption that the average reflectance of the scene tends to achromatic. Then, it can estimate the illuminant color distribution by averaging each channel independently. The Max RGB [20] assumes that the maximum value of each channel is derived from a white patch [18], and further estimates the color of the light source using the maximum values. Gray-world and Max-RGB can be considered as two applications of the Minkowski  $p$ -norm, respectively with  $p = 1$  and  $p = \infty$  [21]. Based on this observation, Finlayson et al. proposed a 'Shades-of-Grey' method that extends the process with changing the  $p$  value to arbitrary, and found that the best results can be obtained by  $p = 6$ . Then Weijer and Gevers proposed Grey-Edge hypothesis [22] that further extends the Minkowski  $p$ -norm based color constancy framework. They presented an assumption that the average edge difference in a scene is achromatic. Based on this assumption, the scene illumination color is extracted from the derivative structure of image channels with the Minkowski  $p$ -norm, different from Shade of grey that derived the scene illumination color from zero-order pixel structure of image channels. Although this approach is computational simply, compared with the previous color correction methods, such as the methods of [23] that relies on the statistics of natural image, it has been shown to obtain more comparable results. Other recent works include [24], which combines adaptive histogram equalization with global color adjustment, and [25], which corrects the underwater image colors using a color transfer method.

### 3. Proposed method

In this section, we first briefly introduce a degradation model for underwater images. Then we propose a novel and effective underwater image color correction method that considering the attenuation level in different wavelength channels, and detail preserved image dehazing method with multi-scale dehazing in gradient domain.

#### 3.1. Underwater optical imaging model

Similar to the degradation model of images captured in atmospheric environments [26], the simplified underwater optical imaging model can be generally formulated as:

$$I^c(x) = J^c(x)t^c(x) + A^c(1 - t^c(x)) \quad (1)$$

where  $x$  denotes the spatial location of each pixel,  $c \in \{R, G, B\}$ .  $I(x)$  indicates the received underwater image,  $J(x)$  is the restored haze-free image,  $t(x)$  denotes the transmission, which describes the proportion of light reaching the camera and  $A$  represents the global backscattered light. In the underwater imaging model, the first component  $D(x) = J(x)t(x)$  indicates the direct transmission, which is used to draw how the scene radiance is attenuated under water. The second part  $L(x) = A(1 - t(x))$  is the backscattered light. To obtain the haze-free image  $J$ , the unknowns  $A$  and  $t$  need to be estimated from the single input image  $I$ , which is essentially an ill-posed problem. Most methods relied on the image degradation model solve this problem by making strong assumptions or priors.

The transmission  $t(x)$  depends on scene depth  $z(x)$  and the light attenuation coefficient  $\beta$  under water:

$$t(x) = e^{-\beta z(x)} \quad (2)$$

Recently, as we can see, most dehazing algorithms [27,28] might be centered on the estimation of transmission as accurate as possible, which is a very challenging problem.

#### 3.2. Attenuation map guided color correction

Underwater images often suffer from color distortion caused by various illumination and medium attenuation properties. In order to improve the visibility of underwater images, it is necessary to rectify the distorted appearance (e.g. green-bluish appearance). Color distortion of underwater images is mainly generated by the selective absorption of light spectrums with depth. Common existing color correction methods based on linear or non-linear transformation like AHE [29], gray-world or linear stretching [12,30] ignore the wavelength-dependent light absorption in underwater imaging, they may not perform well for underwater images, as illustrated in Figs. 3 and 4. For example, in Fig. 3, the red light is absorbed at a higher rate than green-blue light by water, and the intensity of the red channel in the original image is very small. Therefore, an over-correction of the red channel is caused by excessive stretching. Among these traditional color correction methods, we have found through the comprehensive study showed in Figs. 3 and 4 that the simple linear stretching algorithm achieves better visual performance. However, the images corrected by the method suffer from severe red or blue color noises. In the linear stretching method, let  $I_{\max}^c$  and  $I_{\min}^c$  denote the maximum and

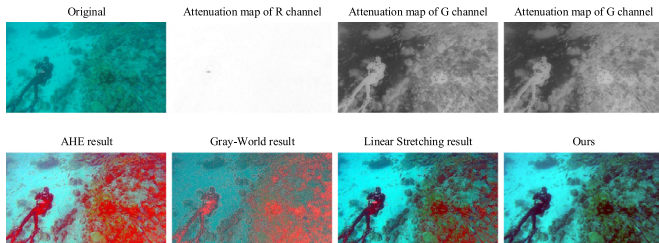


**Fig. 3.** Corrected underwater images generated by several traditional stretching techniques and the proposed approach. According the attenuation map, we found that the red channel suffers from severe attenuation.

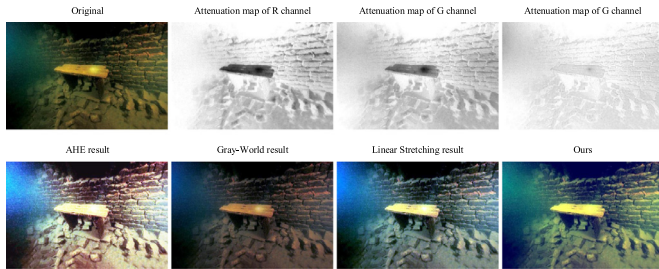


**Fig. 4.** Corrected underwater images generated by several traditional stretching techniques and the proposed approach. According the attenuation map, we found that the blue channel suffers from severe attenuation.

minimum value after cutting 1% of pixels at low and high values of the initial underwater image.

$$I_{CR}^c = 255 * (I^c - I_{\min}^c) / (I_{\max}^c - I_{\min}^c) \quad (3)$$

To address this issue of color noises, an adaptive color correction method is proposed by considering the light attenuation level of each color channel. According to the attenuation level, the color channel will be decided to stretch or compensate. So how to estimate the light attenuation level? Inspired by [25], the light intensity of each color channel should be equal to the original intensity reflected by the object if without considering attenuation, we simply use the difference between the original intensity and the intensity received by the camera to assess the attenuation level of each color light. Attenuation map  $M$  is mathematically represented as:

$$M^c = 1 - (I^c)^\gamma \quad (4)$$

To satisfy the observation characteristics of human eyes, where gamma correction is utilized to correct the received light intensity (we generate our results with the default value of  $\gamma = 1.2$ ). A larger value in the attenuation map indicates a higher attenuation level, such as in Fig. 3, we found that the red channel is highly attenuated according to the attenuation map of R channel. Mathematically, the proposed underwater color correction method is expressed by:

$$I_{CR}^c = \begin{cases} I^c + \alpha(128 - I_{\text{mean}}^c)(1 - I^c), & P^c > 0.7 \\ 255 * (I^c - I_{\min}^c) / (I_{\max}^c - I_{\min}^c), & \text{otherwise} \end{cases} \quad (5)$$

where  $P$  is the probability of values that are more than 0.7 in  $M^c$  and  $\alpha$  is a positive parameter to control the shift range. In the experiments, we find that  $\alpha = 0.5$  produces visually pleasing results. Fig. 5 shows underwater image corrected results generated by several traditional methods and the proposed methods. Now we explain why the proposed color correction method is constructed into Eq. 5. In fact, we introduce the proposed color correction method based on the four following observations/principles:

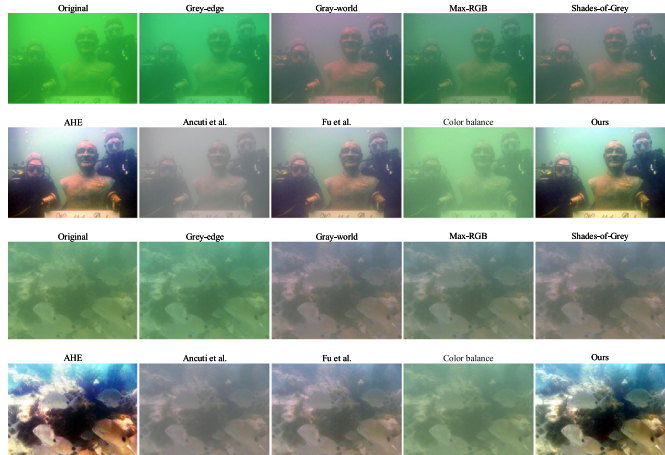


**Fig. 5.** Underwater image corrected results generated by several traditional methods and the underwater image color correction methods of Ancuti et al. [10], Fu et al. [31] and color balance [11].

1. In underwater imaging, R, G and B channels of underwater images may be highly attenuated in some scenes. We first apply the attenuation map to observe the attenuation level and then compensate or stretch channel information by considering the attenuation level of R, G, B channels of the original image, respectively.
2. We use the linear stretching method in the second part of the Eq. (5) considering its advantage of simple implementation and low time consumption. And among these traditional color correction methods, we have found that it can achieve better visual performance through the comprehensive study shown in Figs. 3 and 4.
3. If a single linear stretching method is used to correct the color cast, over-correction may be generated by excessive stretching for some highly attenuated channels. Two examples are reported in Figs. 3 and 4. We propose a compensation method to correct it in terms of the channel with high attenuation. Based on the gray-world assumption, In the proposed compensation strategy, the difference between the mean value of the highly attenuated channel and 128 is used as a criterion to compensate for the highly attenuated channel.
4. For the compensation of each channel, it should focus on compensation for the pixels with small values, and not try to change the pixels that already contain important components.

### 3.3. Transmission estimation based on maximum attenuation identification

Many previous physics-based techniques [32–34] attempted to estimate the transmission by using different assumptions or priors. For instance, the MIP is a prior to estimate the underwater medium transmission by [5]. They think that the red color channel is attenuated at a much higher rate than green or blue. Thus it first calculates the difference between the maximum intensity of the red and that of the green and blue channels:

$$D(x) = \max_{x \in \Omega, c \in r} I^c(x) - \max_{x \in \Omega, c \in b,g} I^c(x) \quad (6)$$

where  $\Omega$  refers to a patch in the image. Large values of  $D(x)$  represent closer scene points whose red light attenuates less than that of further scene points. Then the medium transmission can be estimated by:

$$t(x) = D(x) + \left(1 - \max_x D(x)\right) \quad (7)$$

Although the MIP method is relatively effective for many underwater images. But it is worth mentioning that the red channel attenuates much faster than the green-blue channel is not necessarily correct. The reason for saying so is three-fold: (1) Wavelength attenuation of different colors varies with different water types. In the open ocean, the longer wavelength (i.e., red color) attenuates much faster than the shorter ones. But in the coastal oceans, short wavelength attenuates as strongly as long one [35]. (2) Wavelength attenuation of different colors is highly correlated with the camera sensor, scene radiance and imaging range [36]. It implies that the attenuation of each channel of two images captured by two different cameras in the same scene may be different. (3) The blue channel may be significantly attenuated for some images captured in turbid waters or in places with high concentration of plankton [37,38].

Therefore, to improve the robustness and effectiveness, this paper proposes an adaptive method to estimate the transmission based on maximum attenuation map identification. In the proposed algorithm, the mean value of the attenuation map is used to select the color channel that attenuates at the highest rate. Then inspired by the MIP method, the depth map and transmission map will be estimated. The detailed algorithm is described in **Algorithm 1**.

---

**Algorithm 1** Transmission Estimation Based on Maximum Attenuation Identification.

---

**Input:** Input image  $I^c$

**Output:** Estimated transmission  $t$

1: Estimate attenuation map:

$$M^c = 1 - (I^c)^y$$

2: Determine the color channel that attenuates at the highest rate:

$$c^* = \arg \max_{c \in \{r, g, b\}} (\text{mean}(M^c))$$

3: Estimate depth map:

$$D(x) = \max_{x \in \Omega} I^{c^*}(x) - \max_{x \in \Omega, p \in c - c^*} I^p(x)$$

4: Estimate transmission map:

$$t(x) = D(x) + (1 - \max_x D(x))$$


---

Among it,  $c^*$  is the color channel with the highest attenuated rate while  $c - c^*$  represents the other two channels. Because the MIP and our method are calculated block-by-block, in order to reduce the blocking artifacts, we incorporate the guided filter [41] to refine the final transmission. Examples of transmission estimation via different methods are shown in **Fig. 8**.

**Figs. 6** and **7** show the transmission results generated by MIP and the proposed method, respectively. In **Fig. 6**, the R channel is attenuated at a higher rate than G-B channel. We found that the use of these two methods is effective for the transmission estimation. However, in **Fig. 7**, the B channel is attenuated much faster. At this moment, compared with our method, we obviously found the salient regions of the transmission estimated by MIP is inaccurate. More textures and details of the degraded image are shown in the transmission map yielded by our method, which is very important to accurate haze removal in the following step.

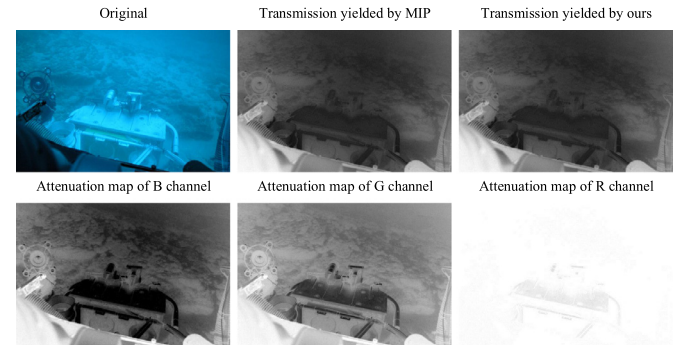


**Fig. 6.** Examples of transmission estimation via the MIP and our method. The R channel of challenging original image is highly absorbed.

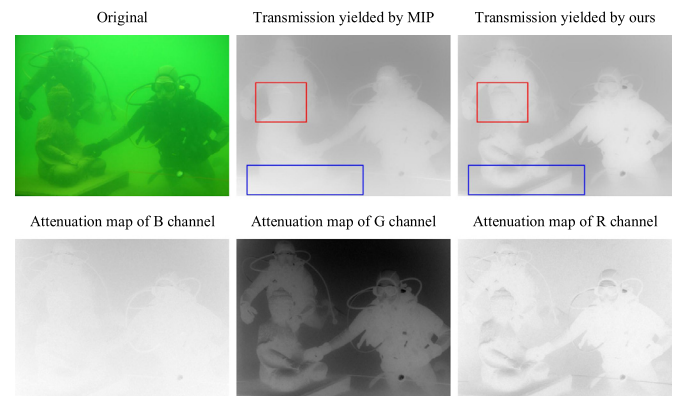


**Fig. 7.** Examples of transmission estimation via the MIP and our method. The B channel of challenging original image is highly absorbed.

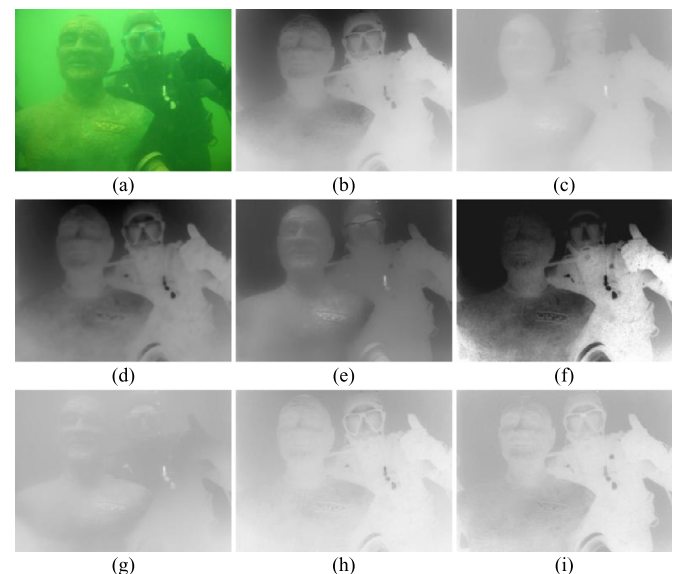


**Fig. 8.** Examples of transmission estimation via different methods. (a) Input image. (b)-(i) are the results of estimated transmission using DCP method [26], UDPCP method [4], GDCP method [39], Blurriness-based method [6], Haze Line method [35], Red-channel method [3], Filter-based method [40] and the proposed method.

### 3.4. Image dehazing via multi-scale edge-preserving decomposition

Based on the degradation model as shown in Eq. (1), we assume that attenuation coefficient  $\beta$  and scene depth  $z(x)$  are constant in a small local patch centered at location  $x$ . Thus transmission  $t$  is uniform, the contrast of the input image (which measured as the

sum of gradient) can be expressed as [42]:

$$\sum_x \|\nabla I(x)\| = t \sum_x \|\nabla J(x)\| \leq \sum_x \|\nabla J(x)\| \quad (8)$$

Note that  $0 \leq t \leq 1$ , which demonstrates that the contrast of hazy images is usually lower, compared with haze-free images. Reduction of the gradient  $\|\nabla J\|$  is highly correlated with the transmission value.

In the proposed method, to avoid subsequent operations affecting the previous recovered color, we first convert the RGB image to LAB color space. Then L channel is decomposed into a base layer and two residual detail layers by a proper edge-preserving decomposition. Owing to this, in different detail layers, the corresponding detail information is captured, with which we can easily restrict the extension of unwanted details while significantly enhancing the desired information. Meanwhile, it worth mentioning that since the back-scattered light contains no detailed information, we think that the base layer contains all the back-scattered light after decomposition. Therefore, to further enhance the details of underwater image, the base layer needs to be cleaned. Finally, the hazy underwater image is restored by blending the cleaned base layer and detail layers which are reconstructed from the processed gradients by solving Poisson equations.

### 3.4.1. Multi-scale edge-preserving decomposition

Generally, multi-scale image decomposition methods determine the appearance of images at multiple scales. We opt an edge-preserving decomposition method, weighted least squares (WLS) [43] in the lightness channel of the LAB color space, to preserve details of the image at multiple scales and avoid artifacts.

A multi-scale representation of lightness channel that consists of a base layer and  $k - 1$  detail layers, is established. The base layer is a coarse version of the lightness channel, and detail layers extract details at progressively finer scales.  $g$  indicates the lightness channel, and  $u^1, \dots, u^{k-1}$  represent progressively coarser version of  $g$ . The coarsest version  $u^{k-1}$  is considered as the base layer  $b$ , and detail layers  $d_i$  can be obtained by subtracting subsequent coarser images. It can be defined as

$$d_i = u^{i-1} - u^i, \quad \text{where } i = 1, \dots, k - 1 \text{ and } u^0 = g \quad (9)$$

Thus, the recovered image can be obtained by the following synthesis transform

$$g = b + \sum_{i=1}^{k-1} d_i \quad (10)$$

In our test, a total number of levels  $k = 3$  is selected. The process of image decomposition employing WLS and the suggested parameters can be shown in Fig. 9.

### 3.4.2. Descattering in base layer

Since the base layer contains the back-scattered light, descattering is used to enhance the base layer. In descattering step, we first utilize the filter-based method [40] to estimate the backscattered light  $L(x)$ .

$$\begin{aligned} L(x) &= \max(\min(B(x), b(x)), 0) \\ \text{with } B(x) &= A(x) - \text{median}_{s_v}(|b - A|)(x) \\ \text{and } A(x) &= \text{median}_{s_v}(b)(x) \end{aligned} \quad (11)$$

where  $s_v$  is the size of the square window in the median filter.  $s_v = 41$  is used in this paper. Then, the descattered base layer  $b'$  is obtained by:

$$b' = b - \varepsilon L \quad (12)$$

where  $\varepsilon$  is a parameter in  $[0, 1]$  that controls the strength of descattering. Considering that underwater images are generally dark, it is suggested to retain some back-scattered light according to various lighting conditions for better display.

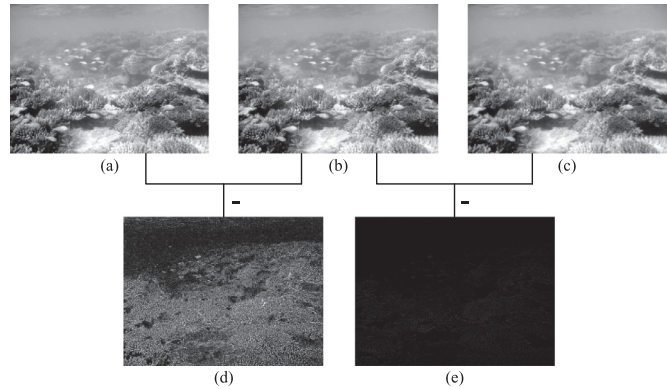


**Fig. 9.** Image decomposition procedure. (a) Lightness channel of the input image in LAB color space. (b)  $u^1$  smoothed with parameters  $\lambda = 0.01$ ,  $\alpha = 0.5$ . (c)  $u^2$  (base layer) smoothed with parameters  $\lambda = 1.00$ ,  $\alpha = 0.5$ . (d) Detail layer  $d_1$  generated from the difference of (a) and (b). (e) Detail layer  $d_2$  generated from the difference of (b) and (c).

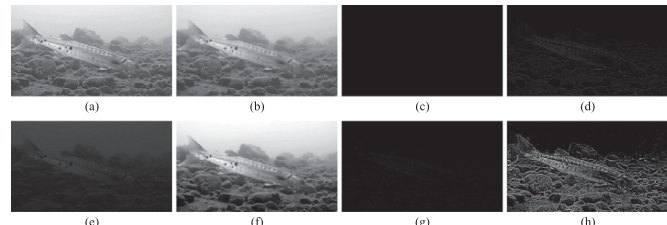


**Fig. 10.** Examples of image dehazing in gradient domain. (a) Input image in L channel. (b)-(d) are the decomposed layers: base layer  $b$ , detail layers  $d_1$  and  $d_2$ . (e) estimated backscattered light. (f)-(h) are the enhanced layers: enhanced base layer  $b'$ , enhanced detail layers  $d'_1$  and  $d'_2$ .

### 3.4.3. Detail enhancement in multi-scale gradient domain

According to Eq. (8), the gradient of the haze-free image is estimated in a straightforward way through dividing the gradient  $\|\nabla I\|$  by the transmission  $t$ . But,  $t$  cannot directly be used as the enhancement factor for the reason that our manipulations of gradients is aimed at residual images, rather than the entire images. Namely,  $\|\nabla I\|$  turns to  $\|\nabla d\|$ . Therefore, here the average of transmission  $\bar{t}$  is allowed to replace  $t$  in Eq. (8). There are two reasons for this: (1)  $\bar{t}$  can also describe the attenuation degree of the hazy image. (2)  $\bar{t}$  can prevent the denominator from infinity close to zero. In addition, to avoid over-enhancement of the detail and amplification of unwanted noise in very hazy regions. We set a lower bounder  $\eta$  ( $\eta = 0.8$  is proposed in this step) on the value of  $\bar{t}$ :

$$\bar{t}(x) = \max(\bar{t}(x), \eta) \quad (13)$$

Then, the manipulations of gradients on detail layers are defined as:

$$\nabla d'_i = \frac{w_i}{\bar{t}} \nabla d_i \quad (14)$$

where  $w_i$  are non-negative parameters used to control the strength of gradient enhancement under different scales. The value of  $w_i$  is determined by the density of haze (in our experiments, we set  $w_1 = 2$ ,  $w_2 = 4$ ).

Finally, reconstructed layers are obtained by solving a Poisson equation [44,45] on the modified gradients (as shown in Fig. 10):

$$d'_i = \text{Restore}(\nabla d'_i) \quad (15)$$

### 3.4.4. Multi-scale image composition

There will produce a descattered base layer  $b'$  and two enhanced detail layers  $d'_1$ ,  $d'_2$  by employing the above steps, and then

the result of final enhanced image for the brightness channel is given in the following way:

$$L_R = b' + S(\delta_1, d'_1) + S(\delta_2, d'_2) \quad (16)$$

with  $S(\delta, x) = 1/(1 + \exp(-\delta x))$

where  $S$  refers to a sigmoid function that is mainly used to prevent the hard clipping produced by significantly boosting the detail layers.  $\delta$  denotes the boosting coefficient which controls the sigmoid curve. All results of our experiment were obtained by the following parameters:  $\delta_1 = \delta_2 = 1$ .

#### 4. Experimental results

In this section, to evaluate the performance, we compare the proposed underwater image enhancement method with several state-of-the-art works: GDCP [39], Retinex-based [12], Fusion-based [10], Haze Line [35], Histogram Prior [7], Blurriness-based [6].

In our experiments, a few dozen underwater images with different light conditions and colors are used as the testing images to verify the performance of the proposed method, and a three-level decomposition ( $base, d_1, d_2$ ) is reconstructed, since we found that three pyramid levels can satisfy the processing requirements of most images. For these images, more levels do not mean significant improvement, but indicates high computational complexity. The qualitative and quantitative evaluations are carried out to assess the performance of different methods. In addition, the proposed method is used to enhance the hazy/foggy/sandy images taken in the atmospheric environment.

##### 4.1. Qualitative comparison

###### 4.1.1. Underwater image dehazing evaluation

In this study, we visually compare the enhancement performance of the proposed method with other methods on real underwater hazy images. As shown in Fig. 11, the effects of scattering can be successfully removed by our algorithm and the visibility of underwater images is effectively restored. Although the qualitative comparison also demonstrates that most of the methods mentioned above are able to achieve better enhancement for underwater hazy images, but due to the accurate estimation of the medium transmission maps and the outperform of the color correction, the results of the proposed method are more natural than the results of other methods. As we can see in Fig. 11, the Fusion-based method performs well in most cases, but the reddish color deviation of the restored image may be introduced due to the inaccurate color correction. The results of Haze Line method generally look darker, and also have color distortion. According to the results obtained from Histogram Prior, there are obvious reddish color shift and artifacts, and the obvious reddish color shift may be generated due to the red channel is over-corrected by excessive stretching. Although Retinex-based method can make more satisfactory dehazed results, but unfortunately, the color of the enhanced image looks particularly weird, and the details are not good enough. GDCP and Blurriness-based methods rely too much on accuracy of the medium transmission estimation, but it is still challenging to generate accurate transmission in the underwater environment. Therefore, the results of their methods are not perform well.

Here, the practical application of the proposed method is verified. As shown in Fig. 12, more practical dehazing results are carried out for real-world underwater hazy images captured in the First Underwater Robot Picking Contest, Zhangzidao, Dalian, China. And it is compared with the mentioned above several state-of-the-art works. It can be found that the results restored by our method are superior to other methods both in color and detail.

###### 4.1.2. Detail-preserving analysis

In underwater image dehazing, the dehazed results with fine-details are important and highly desired for many practical applications (such as object recognition, object tracking, etc.). However, The dehazed results obtained by using existing algorithms tend to be overly smooth with missing fine image details. In this section, we will compare our results with the results yielded by Fusion-based and Blurriness-based methods in terms of detail preserving. The dehazed results from two underwater hazy samples are shown in Fig. 13. As displayed in enlarged regions, our algorithm thoroughly removes haze and naturally restores details.

###### 4.1.3. Underwater dehazing of extreme scenes

We also try to evaluate the dehazing performance of the proposed method for underwater images taken in extreme scenes. Fig. 14 shows two samples derived from the work of Treibitz and Schechner [46]. These images captured in the non-uniform artificial illumination condition suffer from quite low contrast and non-uniformly yellowish. The enhanced images generated using various approaches are reported in Fig. 14. We found that the dehazing performance of our method for the challenging artificially illuminated underwater scenes is inferior to the underwater scenes with reasonable and uniform natural illumination, it may be generated by estimating the backscattered light globally [47].

##### 4.2. Quantitative comparison

To further quantitatively demonstrate the advantages processed by the proposed method, we compare it against six state-of-the-art underwater image enhancement or restoration works via four underwater quality evaluation metrics (Blur [48], PCQI [49], UIQM [50] and UCIQE [51]).

The Blur metric [48] evaluates the image quality in terms of blur perception, and the blur metric ranges from 0 to 1, indicating the best to the worst.

PCQI [49] is used as predicting the human perception of contrast variations, which can be given by:

$$\text{PCQI} = \frac{1}{M} \sum_{i=1}^M q_i(x_i, y_i) q_c(x_i, y_i) q_s(x_i, y_i) \quad (17)$$

where  $M$  is the total number of the patches in the image,  $q_i$ ,  $q_c$  and  $q_s$  are three comparison functions. The higher PCQI values, the better image contrast.

As an underwater image quality measure based on human visual system, UIQM [50] evaluates the quality of an underwater image by its sharpness measure (UISM), colorfulness measure (UICM) and contrast measure (UIConM). Specifically, this assessment can be represented by a linear combination of these three components.

$$\text{UIQM} = c_1 \times \text{UICM} + c_2 \times \text{UISM} + c_3 \times \text{UIConM} \quad (18)$$

where  $c_1$ ,  $c_2$  and  $c_3$  are the scale factors, we set  $c_1 = 0.0282$ ,  $c_2 = 0.2953$ , and  $c_3 = 3.5753$  as the original paper. The higher value of the UIQM stands for the better performance.

In addition, UCIQE [51] is also served as an objective evaluation, it is represented as the linear combination of chroma, saturation and contrast:

$$\text{UCIQE} = m_1 \times \sigma_c + m_2 \times \text{con}_l + m_3 \times \mu_s \quad (19)$$

where  $\sigma_c$  indicates the standard deviation of chroma,  $\text{con}_l$  indicates the contrast of brightness,  $\mu_s$  is the average of saturation, and  $m_1$ ,  $m_2$  and  $m_3$  are weighted factors. We use the recommended weighted factors ( $m_1 = 0.4680$ ,  $m_2 = 0.2745$ , and  $m_3 = 0.2576$ ). The highest UCIQE score means that the method can produce most visually appealing results.



**Fig. 11.** Subjective comparisons on underwater images with different light conditions and colors. From left to right are original images, and the results generated by Fusion-based [10], Haze Line [35], Histogram Prior [7], GDCP [39], Blurriness-based [6], Retinex-based [12] and the proposed method.

**Tables 1** and **2** report the evaluation values of the challenging results shown in **Fig. 11** in terms of Blur, PCQI, UIQM and UCIQE. **Tables 3** and **4** represent the evaluation values of the challenging results shown in **Fig. 12**. The values in bold denote the best results. As described in these four tables, the proposed method performs better in most cases in regard to the values of Blur, PCQI, UIQM. In regard to the values of UCIQE, the proposed method is inferior to Histogram Prior and Haze Line methods as shown in **Tables 1** and **3**. But in **Figs. 11** and **12**, it can be obviously seen that there are artifacts and color casts in these results generated by Histogram Prior and Haze Line methods. What calls for special attentions is that UCIQE did not take the color shift and artifacts into account, which can be observed from Ref. [52].

To assess the robustness and effectiveness of different methods, we also conduct objectively comparison among different underwater image restoration methods on the real-world underwater image enhancement dataset (UIEBD[52] and RUIE[53]).

UIEBD [52] is a large-scale real-world underwater image enhancement benchmark dataset that contains 890 degraded underwater images collected from the Internet. **Fig. 15** (a) lists several

example images of the UIEBD dataset. And the other underwater image dataset RUIE [53] is composed of three subsets, which contains a total of 3930 challenged images of marine life captured in real marine aquaculture environment. In our experiments, two subsets denoted as underwater image quality set and underwater color cast set are used to check the performance of different methods. **Fig. 15** (b) shows some image examples of the RUIE dataset. Here, the average values of four assessment metrics mentioned above are used to quantitatively evaluate the quality of the results restored by different methods. These comparative results are listed in **Tables 5** and **6**. Similarly, The values in bold are the best results. In all assessment metrics, It can be found that the proposed method stands out among the compared methods except for the value of UCIQE.

#### 4.3. Evaluation on synthetic underwater images

In this section, we evaluate the proposed method on synthetic underwater image dataset JWCDN [54] including 1449 samples. **Fig. 16** reports the results yielded using different underwater image

**Table 1**

UIQM and UCIQE values of different methods in Fig. 11.

|             | Fusion-based |        | Haze Line |               | Histogram Prior |               | GDCP   |        | Blurriness-based |        | Retinex |        | Ours          |               |
|-------------|--------------|--------|-----------|---------------|-----------------|---------------|--------|--------|------------------|--------|---------|--------|---------------|---------------|
|             | UIQM         | UCIQE  | UIQM      | UCIQE         | UIQM            | UCIQE         | UIQM   | UCIQE  | UIQM             | UCIQE  | UIQM    | UCIQE  | UIQM          | UCIQE         |
| Fig. 11 (a) | 1.4551       | 0.6474 | 1.5463    | 0.6990        | <b>1.6159</b>   | <b>0.7277</b> | 1.4260 | 0.6133 | 1.3449           | 0.5742 | 1.4579  | 0.6300 | 1.5481        | 0.6827        |
| Fig. 11 (b) | 1.4418       | 0.6279 | 1.1483    | 0.5919        | 1.4483          | 0.6370        | 0.9419 | 0.4146 | 1.0916           | 0.5266 | 1.2843  | 0.5855 | <b>1.6230</b> | <b>0.6387</b> |
| Fig. 11 (c) | 0.9853       | 0.5999 | 1.2202    | 0.6481        | 1.1784          | <b>0.6359</b> | 0.7145 | 0.4778 | 0.9134           | 0.6301 | 0.9081  | 0.5341 | <b>1.7456</b> | 0.6259        |
| Fig. 11 (d) | 1.2500       | 0.6263 | 1.2514    | <b>0.6705</b> | 1.0182          | 0.6495        | 1.0445 | 0.5899 | 0.8735           | 0.5555 | 0.8963  | 0.5634 | <b>1.4784</b> | 0.6034        |
| Fig. 11 (e) | 1.5551       | 0.6048 | 1.5481    | 0.6399        | 1.3234          | <b>0.6440</b> | 0.8669 | 0.5108 | 0.9260           | 0.4885 | 1.1516  | 0.5685 | <b>1.7419</b> | 0.6160        |
| Fig. 11 (f) | 1.4670       | 0.6648 | 1.6005    | 0.6928        | 1.4360          | <b>0.7230</b> | 1.0604 | 0.5724 | 1.0015           | 0.5649 | 1.3591  | 0.6313 | <b>1.7948</b> | 0.6888        |
| Fig. 11 (g) | 1.2871       | 0.5800 | 1.5099    | 0.5998        | 1.4658          | <b>0.6403</b> | 1.3902 | 0.5976 | 0.9414           | 0.4640 | 1.5215  | 0.6253 | <b>1.5929</b> | 0.5926        |
| Fig. 11 (h) | 1.6387       | 0.6449 | 1.6411    | 0.6438        | 1.6815          | <b>0.7155</b> | 1.6568 | 0.6768 | 1.3595           | 0.5876 | 1.5621  | 0.6332 | <b>1.7199</b> | 0.6746        |
| Fig. 11 (i) | 1.5904       | 0.6444 | 1.7244    | 0.6642        | 1.6500          | <b>0.6972</b> | 1.3535 | 0.6045 | 1.4589           | 0.6817 | 1.2372  | 0.5992 | <b>1.9727</b> | 0.6530        |
| Fig. 11 (j) | 1.5099       | 0.6684 | 1.5251    | 0.7368        | 1.4856          | <b>0.7382</b> | 1.3364 | 0.6439 | 1.2081           | 0.5859 | 1.4218  | 0.6549 | <b>1.7253</b> | 0.7003        |

**Table 2**

Blur and PCQI values of different methods in Fig. 11.

|             | Fusion-based |               | Haze Line |        | Histogram Prior |        | GDCP   |        | Blurriness-based |               | Retinex |        | Ours          |               |
|-------------|--------------|---------------|-----------|--------|-----------------|--------|--------|--------|------------------|---------------|---------|--------|---------------|---------------|
|             | Blur         | PCQI          | Blur      | PCQI   | Blur            | PCQI   | Blur   | PCQI   | Blur             | PCQI          | Blur    | PCQI   | Blur          | PCQI          |
| Fig. 11 (a) | 0.3593       | <b>1.2548</b> | 0.3447    | 1.1388 | 0.3444          | 1.2305 | 0.3460 | 1.2051 | 0.3602           | 1.1692        | 0.4043  | 1.0982 | <b>0.2653</b> | 1.2539        |
| Fig. 11 (b) | 0.3834       | <b>1.2429</b> | 0.3889    | 0.7667 | 0.3205          | 1.1465 | 0.3439 | 0.9609 | 0.3953           | 1.0244        | 0.4470  | 1.1274 | <b>0.2994</b> | 1.2195        |
| Fig. 11 (c) | 0.2423       | 0.9965        | 0.2675    | 0.7322 | 0.2166          | 0.9726 | 0.2032 | 0.8044 | 0.2315           | <b>1.0064</b> | 0.3137  | 0.9280 | <b>0.1834</b> | 0.9137        |
| Fig. 11 (d) | 0.2682       | 0.8849        | 0.2786    | 0.5776 | 0.3120          | 0.7352 | 0.2969 | 0.6636 | 0.3316           | 0.6457        | 0.3902  | 0.7271 | <b>0.1528</b> | <b>1.3627</b> |
| Fig. 11 (e) | 0.1849       | 1.0166        | 0.2174    | 0.6054 | 0.2324          | 0.8125 | 0.2585 | 0.6796 | 0.2465           | 0.6732        | 0.2995  | 0.7479 | <b>0.1381</b> | 1.1423        |
| Fig. 11 (f) | 0.3457       | 1.1601        | 0.3046    | 0.9222 | 0.3467          | 1.0894 | 0.3435 | 1.0102 | 0.3590           | 0.9860        | 0.4013  | 1.0419 | <b>0.2253</b> | 1.3043        |
| Fig. 11 (g) | 0.5255       | 1.1693        | 0.3982    | 0.8387 | <b>0.3118</b>   | 1.0882 | 0.4549 | 1.0623 | 0.4627           | 1.0294        | 0.3245  | 1.0484 | 0.3465        | <b>1.2294</b> |
| Fig. 11 (h) | 0.2484       | 1.2347        | 0.2582    | 1.0965 | 0.2439          | 1.1600 | 0.2372 | 1.2060 | 0.2648           | 0.9839        | 0.3107  | 0.9500 | <b>0.1830</b> | 1.3576        |
| Fig. 11 (i) | 0.2432       | 1.2169        | 0.2195    | 1.0447 | 0.2139          | 1.0569 | 0.2202 | 1.0390 | 0.2287           | 1.1117        | 0.3114  | 0.9223 | <b>0.1724</b> | 1.3178        |
| Fig. 11 (j) | 0.2781       | <b>1.2097</b> | 0.2712    | 0.8129 | 0.2793          | 1.0309 | 0.2768 | 1.1163 | 0.2977           | 1.0217        | 0.3437  | 0.9413 | <b>0.2181</b> | 1.1688        |

**Table 3**

UIQM and UCIQE values of different methods in Fig. 12.

|             | Fusion-based |        | Haze Line     |               | Histogram Prior |               | GDCP   |        | Blurriness-based |        | Retinex |        | Ours          |        |
|-------------|--------------|--------|---------------|---------------|-----------------|---------------|--------|--------|------------------|--------|---------|--------|---------------|--------|
|             | UIQM         | UCIQE  | UIQM          | UCIQE         | UIQM            | UCIQE         | UIQM   | UCIQE  | UIQM             | UCIQE  | UIQM    | UCIQE  | UIQM          | UCIQE  |
| Fig. 12 (a) | 1.5534       | 0.6142 | <b>1.6981</b> | 0.6342        | 1.6147          | <b>0.6732</b> | 1.5835 | 0.5924 | 1.4886           | 0.5791 | 1.5076  | 0.5834 | 1.6469        | 0.6265 |
| Fig. 12 (b) | 1.4976       | 0.6268 | 1.5638        | 0.6285        | 1.4960          | <b>0.6731</b> | 1.5415 | 0.6532 | 1.4677           | 0.6034 | 1.4181  | 0.5905 | <b>1.6553</b> | 0.6286 |
| Fig. 12 (c) | 1.6721       | 0.6670 | <b>1.8493</b> | 0.6397        | 1.7681          | <b>0.6901</b> | 1.2035 | 0.5277 | 1.1987           | 0.5272 | 1.5679  | 0.5930 | 1.6435        | 0.6174 |
| Fig. 12 (d) | 1.3921       | 0.5942 | 1.4191        | <b>0.6490</b> | 1.4712          | 0.6374        | 1.0109 | 0.4253 | 1.2671           | 0.5770 | 1.3904  | 0.5786 | <b>1.6377</b> | 0.6235 |
| Fig. 12 (e) | 1.3319       | 0.6802 | 1.3419        | 0.6704        | 1.3576          | <b>0.7288</b> | 1.1847 | 0.6092 | 1.0020           | 0.5640 | 1.3479  | 0.6512 | <b>1.4920</b> | 0.6878 |

**Table 4**

Blur and PCQI values of different methods in Fig. 12.

|             | Fusion-based  |               | Haze Line |        | Histogram Prior |        | GDCP   |        | Blurriness-based |        | Retinex |        | Ours          |               |
|-------------|---------------|---------------|-----------|--------|-----------------|--------|--------|--------|------------------|--------|---------|--------|---------------|---------------|
|             | Blur          | PCQI          | Blur      | PCQI   | Blur            | PCQI   | Blur   | PCQI   | Blur             | PCQI   | Blur    | PCQI   | Blur          | PCQI          |
| Fig. 12 (a) | 0.2545        | 1.3484        | 0.2094    | 1.0420 | 0.2215          | 1.2703 | 0.2221 | 1.2055 | 0.2222           | 1.1981 | 0.2966  | 1.1637 | <b>0.2066</b> | <b>1.4769</b> |
| Fig. 12 (b) | 0.2964        | 1.3054        | 0.2383    | 0.8185 | 0.2711          | 1.1957 | 0.2657 | 1.1664 | 0.2710           | 1.1663 | 0.3593  | 1.0946 | <b>0.2203</b> | <b>1.3629</b> |
| Fig. 12 (c) | <b>0.1781</b> | 1.2285        | 0.1848    | 1.1809 | 0.1841          | 1.2203 | 0.2386 | 1.0906 | 0.2455           | 1.1293 | 0.2759  | 1.2426 | 0.2264        | <b>1.3917</b> |
| Fig. 12 (d) | 0.3321        | <b>1.2822</b> | 0.3046    | 1.1764 | 0.3137          | 1.1895 | 0.2908 | 0.8902 | 0.3266           | 1.2001 | 0.3824  | 1.0553 | <b>0.2465</b> | 1.2542        |
| Fig. 12 (e) | 0.3895        | 1.1290        | 0.3846    | 1.0887 | 0.3553          | 1.1435 | 0.3693 | 1.1098 | 0.3959           | 1.0541 | 0.4185  | 1.0857 | <b>0.3186</b> | <b>1.1507</b> |

enhancement methods on two samples from JWCDN. Comparing with other methods, it can be observed that the images generated by the proposed method provides sharper contours with less color distortion, which resembles the ground truth.

Since the ground truth images are available in the synthetic dataset JWCDN, which enables us to quantitatively check the performance using full-reference image quality assessments MSE, PSNR, SSIM [55] and PCQI [49]. In terms of MSE and PSNR metrics, the lower MSE (higher PSNR) indicates the result is closer to the ground truth image in regard of image content. SSIM metric measures the visual impact of an image including luminance, contrast and structure. A higher SSIM value means a better result of enhancement. The average quantitative scores conducted on JWCDN are listed in Table 7. The values in bold denotes the best results. It can be found that the best results are obtained by the proposed method. In addition, we observe that the SSIM val-

ues of GDCP and Blurriness-based are negative, due to the negative correlation coefficients between the results and the ground truth images.

Overall, we conclude that the proposed approach generally results in better perceptual quality, with sufficient enhancement of the global contrast, the color and the details.

#### 4.4. Ablation study

To demonstrate the effectiveness of each component in the proposed method, we conduct an ablation study involving the following experiments on UIEBD and RUIE : (a) the proposed method without color correction (-w/o CC), (b) the proposed without detail preserved dehazing (-w/o DPD), (c) the proposed method without descattering in the base layer (-w/o DIBL). Fig. 17 shows an example about visual comparisons. From Fig. 17, the following observa-

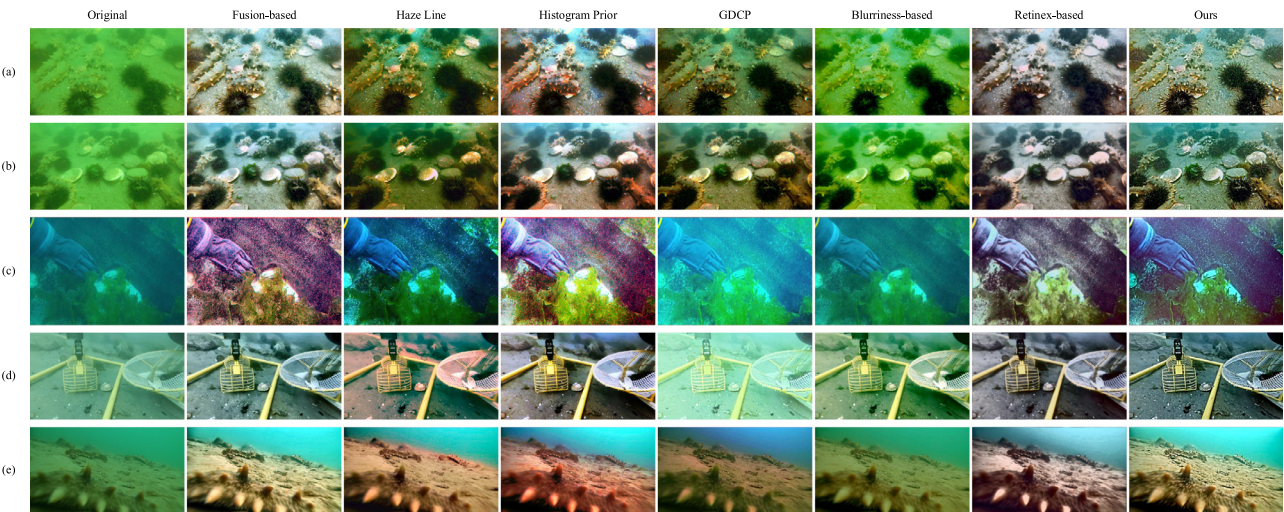


**Fig. 12.** More practical results on underwater images captured in real marine aquaculture environment. From left to right are original images, and the results generated by Fusion-based [10], Haze Line [35], Histogram Prior [7], GDCP [39], Bluriness-based [6], Retinex-based [12] and the proposed method.



**Fig. 13.** Experimental results about detail preserving among the images yielded by different underwater image enhancement methods. (a) Original underwater images with two detail enlarged views. The restored results yield by: (b) Blurriness-based method [6], (c) Fusion-based method [10], (d) the proposed method.

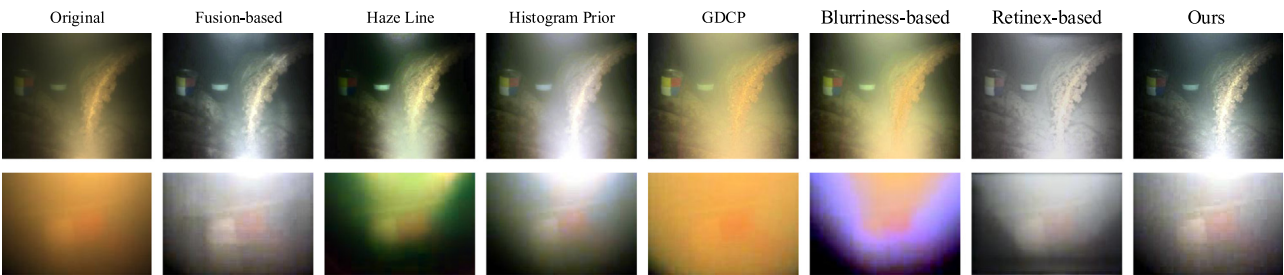


**Fig. 14.** Underwater dehazing of extreme scenes characterized by the nonuniform illumination condition.

tions can be found: 1) More details can be obtained in the image yielded by ours-w/o CC, but the degradation of color has not been effectively improved. The use of color correction is able to better generate realistic colors. 2) Ours-w/o DPD makes some desirable colors, however image details are not obtained. The use of detail preserved dehazing method is able to preserve details while making desirable colors. 3) Ours-w/o DIBL leads to a lack of image lo-

cal details. The image generated by the proposed method obtains a better visibility.

The quantitative results evaluated for the various configurations on UIEBD and RUIE datasets are tabulated in [Table 8](#). Comparing with other configurations, the proposed method obtains higher values in terms of Blur, UIQM, PCQI and UCIQE metrics, which demonstrates the effectiveness of each component.



**Fig. 15.** Example images from (a) UIEBD [52] and (b) RUIE [53].

**Table 5**

Quantitative results in terms of the average values of Blur UIQM, PCQI and UCIQE on UIEBD dataset.

| Method           | Blur          | UIQM          | PCQI          | UCIQE         |
|------------------|---------------|---------------|---------------|---------------|
| Fusion-based     | 0.2841        | 1.5256        | 1.2104        | 0.6399        |
| Haze Line        | 0.2935        | 1.5134        | 0.9079        | 0.6558        |
| Histogram Prior  | 0.2666        | 1.5429        | 1.1281        | <b>0.6777</b> |
| GDCP             | 0.2657        | 1.4266        | 1.0450        | 0.5983        |
| Blurriness-based | 0.2826        | 1.3733        | 1.0744        | 0.5989        |
| Retinex-based    | 0.3079        | 1.2641        | 0.9002        | 0.5394        |
| Ours             | <b>0.2153</b> | <b>1.6266</b> | <b>1.2688</b> | 0.6496        |

**Table 6**

Quantitative results in terms of the average values of Blur UIQM, PCQI and UCIQE on RUIE dataset.

| Method           | Blur          | UIQM          | PCQI          | UCIQE         |
|------------------|---------------|---------------|---------------|---------------|
| Fusion-based     | 0.3339        | 1.5129        | 1.2936        | 0.6243        |
| Haze Line        | 0.3340        | 1.4874        | 1.0470        | 0.6292        |
| Histogram Prior  | 0.3368        | 1.5082        | 1.2393        | <b>0.6732</b> |
| GDCP             | 0.3241        | 1.3047        | 1.0494        | 0.5387        |
| Blurriness-based | 0.3428        | 1.1673        | 1.1085        | 0.5179        |
| Retinex-based    | 0.3813        | 1.4698        | 1.1401        | 0.6041        |
| Ours             | <b>0.2743</b> | <b>1.5610</b> | <b>1.3436</b> | 0.6116        |

**Table 7**

Quantitative results in terms of the average values of MSE, PSNR, SSIM and PCQI on JWCDN dataset.

| Method           | MSE           | PSNR           | SSIM          | PCQI          |
|------------------|---------------|----------------|---------------|---------------|
| Fusion-based     | 1.6684        | 17.7235        | 0.6359        | 0.8314        |
| Haze Line        | 4.3447        | 12.5178        | 0.0971        | 0.5199        |
| Histogram Prior  | 1.8129        | 17.0985        | 0.6095        | 0.7406        |
| GDCP             | 7.3493        | 10.0521        | -0.0079       | 0.6061        |
| Blurriness-based | 5.3132        | 11.4515        | -0.0652       | 0.5845        |
| Retinex-based    | 1.6688        | 16.9532        | 0.5295        | 0.6590        |
| Ours             | <b>1.1644</b> | <b>18.3629</b> | <b>0.6702</b> | <b>0.9216</b> |

#### 4.5. Other applications in the atmosphere

Although the goal of our approach is to improve the restored quality of underwater hazy images, in this part, the proposed approach is still attempted to restore the degraded images taken in adverse weather and special circumstances (hazy, foggy, sandy and etc.), as shown in Fig. 18. It can be found that the results generated via the proposed method look more visually pleasing.



**Fig. 17.** Results yielded using different components. The bottom two rows are the two detail enlarged views derived from the enhanced results presented in the top row.



**Fig. 18.** Results yielded on hazy, foggy and sandy images. Top row is the original images, and the bottom row is the enhanced results by the proposed method.

**Table 8**

Ablation study on the two real-world underwater image datasets UIEBD and RUIE.

| Datasets | Methods   | Blur          | UIQM          | PCQI          | UCIQE         |
|----------|-----------|---------------|---------------|---------------|---------------|
| UIEBD    | -w/o CC   | 0.2250        | 1.5418        | 1.2024        | 0.5621        |
|          | -w/o DPD  | 0.2896        | 1.4127        | 1.0970        | 0.6450        |
|          | -w/o DIBL | 0.2208        | 1.6044        | <b>1.3047</b> | 0.6496        |
|          | Ours      | <b>0.2153</b> | <b>1.6266</b> | 1.2688        | <b>0.6496</b> |
| RUIE     | -w/o CC   | 0.2829        | 1.4198        | 1.1771        | 0.4535        |
|          | -w/o DPD  | 0.3470        | 1.3783        | 1.1709        | <b>0.6304</b> |
|          | -w/o DIBL | 0.2814        | 1.5219        | 1.3276        | 0.6200        |
|          | Ours      | <b>0.2743</b> | <b>1.5610</b> | <b>1.3436</b> | 0.6116        |

#### 5. Conclusion

In this paper, we introduced a novel dehazing method for single underwater image based on color correction and multi-scale gradient domain detail enhancement. First, to address the color distortion, a simple yet effective color correcting algorithm based on piece-wise linear transformation is proposed. Comparative results with other correcting measures demonstrate the proposed correcting algorithm achieves good visual performance in regard to restoring the color tone. Then, a multi-scale gradient domain detail enhancement method is presented to compensate for the lost details meanwhile can eliminate the effects of haze. Experi-

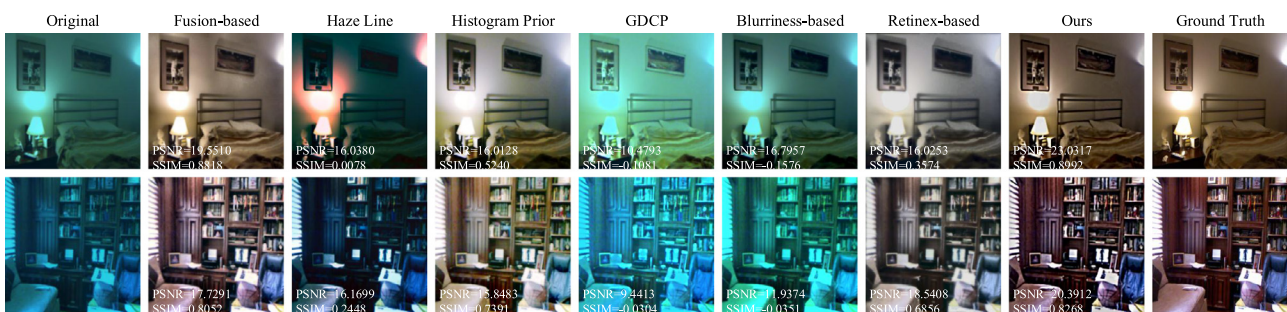


**Fig. 16.** Enhanced results yielded using different underwater image enhancement methods on two samples from JWCDN.

ments tested on underwater images with various light conditions and colors show that the proposed dehazing measure can produce promising results with removing color casts and preserving details when comparing with other state-of-the-art underwater image dehazing methods.

Despite of the good performance, the proposed method nevertheless suffers from some limitations. It still exhibits significant drawback for addressing underwater images taken under several challenging scenes (such as non-uniform artificial illumination and high turbidity water). In addition, the expensive computation complexity may be occurred in the proposed method. For future work, we intend to overcome these limitations.

## Declaration of Competing Interest

We wish to confirm that there are no known conflicts of interest associated with this publication and there has been no significant financial support for this work that could have influenced its outcome.

## CRediT authorship contribution statement

**Zheng Liang:** Writing - original draft, Writing - review & editing, Conceptualization, Methodology. **Yafei Wang:** Writing - original draft, Writing - review & editing, Conceptualization, Methodology. **Xueyan Ding:** Validation, Data curation. **Zetian Mi:** Conceptualization, Writing - review & editing, Funding acquisition. **Xianping Fu:** Supervision, Project administration, Funding acquisition.

## Acknowledgment

The authors would like to thank Haiyan Zhuo for her scientific collaboration in this research work. The authors sincerely thank the editors and anonymous reviewers for the very helpful and kind comments to assist in improving the presentation of our paper. This work was supported in part by the National Natural Science Foundation of China Grant 61802043 and Grant 61370142, by the Liaoning Revitalization Talents Program Grant XLYC1908007, by the Foundation of Liaoning Key Research and Development Program Grant 201801728, by the Fundamental Research Funds for the Central Universities Grant 3132016352 and Grant 3132020215, by the Dalian Science and Technology Innovation Fund 2018J12GX037 and 2019J11CY001.

## References

- [1] J.Y. Chiang, Y.-C. Chen, Underwater image enhancement by wavelength compensation and dehazing, *IEEE Trans. Image Process.* 21 (4) (2012) 1756–1769.
- [2] H. Wen, Y. Tian, T. Huang, W. Gao, Single underwater image enhancement with a new optical model, in: Proc. IEEE International Symposium on Circuits and Systems (ISCAS), IEEE, 2013, pp. 753–756.
- [3] A. Galdran, D. Pardo, A. Picón, A. Alvarez-Gila, Automatic red-channel underwater image restoration, *J. Vis. Commun. Image Represent.* 26 (2015) 132–145.
- [4] P. Drews, E. Nascimento, F. Moraes, S. Botelho, M. Campos, Transmission estimation in underwater single images, in: Proc. IEEE International Conference on Computer Vision Workshops (ICCVW), 2013, pp. 825–830.
- [5] N. Carlevaris-Bianco, A. Mohan, R.M. Eustice, Initial results in underwater single image dehazing, in: MTS/IEEE Oceans 2010 Seattle, IEEE, 2010, pp. 1–8.
- [6] Y.-T. Peng, P.C. Cosman, Underwater image restoration based on image blurriness and light absorption, *IEEE Trans. Image Process.* 26 (4) (2017) 1579–1594.
- [7] C.-Y. Li, J.-C. Guo, R.-M. Cong, Y.-W. Pang, B. Wang, Underwater image enhancement by dehazing with minimum information loss and histogram distribution prior, *IEEE Trans. Image Process.* 25 (12) (2016) 5664–5677.
- [8] Y. Wang, H. Liu, L.-P. Chau, Single underwater image restoration using adaptive attenuation-curve prior, *IEEE Trans. Circ. Syst. I Regul. Pap.* 65 (3) (2017) 992–1002.
- [9] A.S.A. Ghani, N.A.M. Isa, Underwater image quality enhancement through integrated color model with rayleigh distribution, *Appl. Soft Comput.* 27 (2015) 219–230.
- [10] C. Ancuti, C.O. Ancuti, T. Haber, P. Bekaert, Enhancing underwater images and videos by fusion, in: Proc. IEEE Conference on Computer Vision and Pattern Recognition (CVPR), IEEE, 2012, pp. 81–88.
- [11] C.O. Ancuti, C. Ancuti, C. De Vleeschouwer, P. Bekaert, Color balance and fusion for underwater image enhancement, *IEEE Trans. Image Process.* 27 (1) (2017) 379–393.
- [12] X. Fu, P. Zhuang, Y. Huang, Y. Liao, X.-P. Zhang, X. Ding, A retinex-based enhancing approach for single underwater image, in: Proc. IEEE International Conference on Image Processing (ICIP), IEEE, 2014, pp. 4572–4576.
- [13] E.H. Land, J.J. McCann, Lightness and retinex theory, *JOSA* 61 (1) (1971) 1–11.
- [14] Y. Li, H. Lu, J. Li, X. Li, Y. Li, S. Serikawa, Underwater image de-scattering and classification by deep neural network, *Comput. Electr. Eng.* 54 (2016) 68–77.
- [15] J. Li, K.A. Skinner, R.M. Eustice, M. Johnson-Roberson, WaterGAN: unsupervised generative network to enable real-time color correction of monocular underwater images, *IEEE Robot. Autom. Lett.* 3 (1) (2018) 387–394.
- [16] S. Anwar, C. Li, F. Porikli, Deep underwater image enhancement, *arXiv:1807.03528* (2018).
- [17] Y. Guo, H. Li, P. Zhuang, Underwater image enhancement using a multiscale dense generative adversarial network, *IEEE J. Ocean. Eng.* (2019).
- [18] M. Ebner, *Color Constancy*, 7, John Wiley & Sons, 2007.
- [19] G. Buchsbaum, A spatial processor model for object colour perception, *J. Frankl. Inst.* 310 (1) (1980) 1–26.
- [20] E.H. Land, The retinex theory of color vision, *Sci. Am.* 237 (6) (1977) 108–129.
- [21] G.D. Finlayson, E. Trezzi, Shades of gray and colour constancy, in: *Color and Imaging Conference*, 2004, Society for Imaging Science and Technology, 2004, pp. 37–41.
- [22] J. Van De Weijer, T. Gevers, A. Gijsenij, Edge-based color constancy, *IEEE Trans. Image Process.* 16 (9) (2007) 2207–2214.
- [23] A. Gijsenij, T. Gevers, Color constancy using natural image statistics and scene semantics, *IEEE Trans. Pattern Anal. Mach. Intell.* 33 (4) (2011) 687–698.
- [24] C.O. Ancuti, C. Ancuti, T. Haber, P. Bekaert, Fusion-based restoration of the underwater images, in: Proc. IEEE International Conference on Image Processing (ICIP), IEEE, 2011, pp. 1557–1560.
- [25] C.O. Ancuti, C. Ancuti, C. De Vleeschouwer, R. Garcia, Locally adaptive color correction for underwater image dehazing and matching, in: Proc. IEEE Conference on Computer Vision and Pattern Recognition Workshops (CVPRW), 2017, pp. 1–9.
- [26] K. He, J. Sun, X. Tang, Single image haze removal using dark channel prior, *IEEE Trans. Pattern Anal. Mach. Intell.* 33 (12) (2011) 2341–2353.
- [27] Y. Wang, H. Liu, L.-P. Chau, Single underwater image restoration using adaptive attenuation-curve prior, *IEEE Trans. Circ. Syst. I Regul. Pap.* 65 (3) (2018) 992–1002.
- [28] H.-H. Chang, C.-Y. Cheng, C.-C. Sung, Single underwater image restoration based on depth estimation and transmission compensation, *IEEE J. Ocean. Eng.* 99 (2018) 1–20.
- [29] S.M. Pizer, E.P. Amburn, J.D. Austin, R. Cromartie, A. Geselowitz, T. Greer, B. ter Haar Romeny, J.B. Zimmerman, K. Zuiderveld, Adaptive histogram equalization and its variations, *Comput. Vis. Graph. Image Process.* 39 (3) (1987) 355–368.
- [30] J. Ao, C. Ma, Adaptive stretching method for underwater image color correction, *Int. J. Pattern Recognit. Artif. Intell.* 32 (2) (2018) 1854001.
- [31] X. Fu, Z. Fan, M. Ling, Y. Huang, X. Ding, Two-step approach for single underwater image enhancement, in: Proc. International Symposium on Intelligent Signal Processing and Communication Systems (ISPACS), IEEE, 2017, pp. 789–794.
- [32] J.R. Paulo Drews, E. Nascimento, F. Moraes, S. Botelho, M. Campos, Transmission estimation in underwater single images, in: Proc. IEEE International Conference on Computer Vision Workshops (ICCVW), 2013.
- [33] Y.-T. Peng, X. Zhao, P.C. Cosman, Single underwater image enhancement using depth estimation based on blurriness, in: Proc. IEEE International Conference on Image Processing (ICIP), IEEE, 2015, pp. 4952–4956.
- [34] X. Zhao, T. Jin, S. Qu, Deriving inherent optical properties from background color and underwater image enhancement, *Ocean Eng.* 94 (2015) 163–172.
- [35] D. Berman, T. Treibitz, S. Avidan, Diving into haze-lines: color restoration of underwater images, in: Proc. British Machine Vision Conference (BMVC), 1, 2017.
- [36] D. Akkaynak, T. Treibitz, A revised underwater image formation model, in: Proc. IEEE Conference on Computer Vision and Pattern Recognition (CVPR), 2018, pp. 6723–6732.
- [37] H. Lu, Y. Li, L. Zhang, S. Serikawa, Contrast enhancement for images in turbid water, *JOSA A* 32 (5) (2015) 886–893.
- [38] H. Lu, Y. Li, X. Xu, J. Li, Z. Liu, X. Li, J. Yang, S. Serikawa, Underwater image enhancement method using weighted guided trigonometric filtering and artificial light correction, *J Vis Commun Image Represent* 38 (2016) 504–516.
- [39] Y.-T. Peng, K. Cao, P.C. Cosman, Generalization of the dark channel prior for single image restoration, *IEEE Trans. Image Process.* 27 (6) (2018) 2856–2868.
- [40] J.-P. Tarel, N. Hautiere, Fast visibility restoration from a single color or gray level image, in: Proc. IEEE International Conference on Computer Vision (ICCV), IEEE, 2009, pp. 2201–2208.
- [41] K. He, J. Sun, X. Tang, Guided image filtering, in: European Conference on Computer Vision (ECCV), Springer, 2010, pp. 1–14.
- [42] E. Park, J.-Y. Sim, Gradient-based contrast enhancement and color correction for underwater images, in: 2017 Asia-Pacific Signal and Information Processing Association Annual Summit and Conference (APSIPA ASC), IEEE, 2017, pp. 1444–1447.
- [43] Z. Farbman, R. Fattal, D. Lischinski, Edge-preserving decompositions for multi-scale tone and detail manipulation, *ACM Trans. Graph.* 27 (3) (2008) 1.
- [44] R. Fattal, D. Lischinski, M. Werman, Gradient domain high dynamic range compression, in: Conference on Computer Graphics & Interactive Techniques, 2002.

- [45] Z. Mi, Z. Liang, Y. Wang, X. Fu, Z. Chen, Multi-scale gradient domain underwater image enhancement, in: 2018 OCEANS-MTS/IEEE Kobe Techno-Oceans (OTO), IEEE, 2018, pp. 1–5.
- [46] T. Treibitz, Y.Y. Schechner, Active polarization descattering, *IEEE Trans. Pattern Anal. Mach. Intell.* 31 (3) (2008) 385–399.
- [47] C. Ancuti, C.O. Ancuti, C. De Vleeschouwer, R. Garcia, A.C. Bovik, Multi-scale underwater descattering, in: 2016 23rd International Conference on Pattern Recognition (ICPR), IEEE, 2016, pp. 4202–4207.
- [48] F. Crete, T. Dolmire, P. Ladret, M. Nicolas, The blur effect: perception and estimation with a new no-reference perceptual blur metric, in: Human Vision and Electronic Imaging XII, 6492, International Society for Optics and Photonics, 2007, p. 649201.
- [49] S. Wang, K. Ma, H. Yeganeh, Z. Wang, W. Lin, A patch-structure representation method for quality assessment of contrast changed images, *IEEE Signal Process. Lett.* 22 (12) (2015) 2387–2390.
- [50] K. Panetta, C. Gao, S. Agaian, Human-visual-system-inspired underwater image quality measures, *IEEE J. Ocean. Eng.* 41 (3) (2016) 541–551.
- [51] M. Yang, A. Sowmya, An underwater color image quality evaluation metric, *IEEE Trans. Image Process.* 24 (12) (2015) 6062–6071.
- [52] C. Li, C. Guo, W. Ren, R. Cong, J. Hou, S. Kwong, D. Tao, An underwater image enhancement benchmark dataset and beyond, [arXiv:1901.05495](https://arxiv.org/abs/1901.05495) (2019).
- [53] R. Liu, M. Hou, X. Fan, Z. Luo, Real-world underwater enhancement: challenging, benchmark and efficient solutions, [arXiv:1901.05320](https://arxiv.org/abs/1901.05320) (2019).
- [54] X. Ding, Y. Wang, Y. Yan, Z. Liang, Z. Mi, X. Fu, Jointly adversarial network to wavelength compensation and dehazing of underwater images, [arXiv:1907.05595](https://arxiv.org/abs/1907.05595) (2019).
- [55] Z. Wang, A.C. Bovik, H.R. Sheikh, E.P. Simoncelli, et al., Image quality assessment: from error visibility to structural similarity, *IEEE Trans. Image Process.* 13 (4) (2004) 600–612.



**Zheng Liang** is currently pursuing the Ph.D. degree in computer science and technology from Dalian Maritime University, China. His current research interests focus on image processing and machine learning.



**Yafei Wang** received the Ph.D. degree in electronics science and technology from Dalian University of Technology, Dalian, China, in 2018. He is currently a Postdoctoral Research Fellow with Dalian Maritime University, Dalian, China. His current research interests include image processing, computer vision, and machine learning.



**Xueyan Ding** received the B.S. and M.S. degrees in computer science and technology from Dalian Maritime University, China, in 2015 and 2018, respectively, where she is currently pursuing the Ph.D. degree. Her current research interests focus on image processing and machine learning.



**Zetian Mi** received the B.S. and Ph.D. degrees in computer science and technology from Sichuan University, Chengdu, China, in 2012 and 2017, respectively. She is now a Lecturer with Dalian Maritime University, Dalian, China. Her current research interests focus on image processing and machine learning.



**Xianping Fu** received the Ph.D. degree in communication and information system from Dalian Maritime University, Dalian, China, in 2005. From 2008 to 2009, he was a Postdoctoral Fellow with Schepens Eye Research Institute, Harvard Medical School, Boston, MA. He is currently a Professor with Information Science and Technology College, Dalian Maritime University. His research interests include perception of natural scenes in engineering systems, including multimedia, image/video processing, and object recognition.